Unlocking the Potential of Battery Research

Unlocking the Potential
of Battery Research:
Advanced Characterization
of Cell Components

PerkinElmer
For the Better

Wiley Analytical Science

A New Expert Insight.
Download for free.

Battery research is essential to meet the growing demand for reliable, efficient, cost-effective energy storage solutions.

This expert insight presents recent research on solid polymer electrolytes (SPEs), recycling methods for lithium-ion batteries (LIBs), and cathode degradation during extreme fast charging (XFC) of electric vehicles.

PerkinElmer
For the Better

WILEY

RESEARCH ARTICLE

ADVANCED
ENERGY & SUSTAINABILITY
RESEARCH
Open Access

www.advenergysustres.com

Highly Conductive Charge Transport Layers Impair Charge Extraction Selectivity in Thin-Film Solar Cells

Mathias Nyman,* Christian Ahläng, Staffan Dahlström, Manasi Pranav, Johannes Benduhn, Syeda Qudsia, Jan-Henrik Smått, Donato Spoltore, and Ronald Österbacka

In thin-film photovoltaics, such as organic and perovskite solar cells, charge extraction selectivity is crucial. In order to improve selectivity, charge transporting layers (doped and undoped) are frequently used; however, it is not well understood how a charge transporting layer should be designed in order to ensure efficient extraction of majority carriers while blocking minority carriers. This study clarifies how well charge transporting layers with varying majority carrier conductivities block minority carriers. The charge extraction by a linearly increasing voltage technique is used to determine the surface recombination velocity of minority carriers in model system devices with varying majority carrier conductivity in the transporting layer. The results show that transporting layers with high conductivity for majority carriers do not block minority carriers—at least not at operating voltages close to or above the built-in voltage, due to direct bimolecular recombination across the transporting layer–absorber layer interface. Design principles are furthermore discussed and proposed to achieve selective charge extraction in thin-film solar cells using charge transporting layers.

1. Introduction

Solar cells based on low-mobility semiconductors such as organic polymers and small molecules and hybrid organic–inorganic perovskites hold great potential for future low-cost energy production. Due to improved understanding of the efficiency limiting factors and better performing materials, the field has seen a rapid increase in power conversion efficiencies in recent years.[1] The improved performance can partly be attributed to reduced charge carrier recombination in the bulk of the active layers observed in many systems (see refs. [2–4] and references therein). As bulk recombination decreases, surface recombination, i.e., the recombination of minority carriers at the electrodes (holes at the cathode and electrons at the anode), becomes an increasingly important loss mechanism.

In order to ensure selective extraction of charge carriers, i.e., holes at the anode and electrons at the cathode, charge selective interlayers are typically introduced. There are plenty of materials available for use as charge selective interlayers, such as doped and undoped organic semiconductors and various metal oxides, to name a few.[5] The thicknesses of the selective layers can vary greatly, from subnanometer insulating layers to doped layers 100 nm or thicker. The importance of charge selective interlayers in solar cells can hardly be exaggerated; improving the selectivity of contacts has improved both open circuit voltage (V_{OC}) and fill factor (FF).[6–10] It has been suggested that highly selective interlayers can be sufficient to provide a diode behavior to the device. In this case, there would be no need for a built-in voltage (V_{bi}).[11]

M. Nyman, C. Ahläng, S. Dahlström, R. Österbacka
Physics, Faculty of Science and Engineering
Åbo Akademi University
Henriksgatan 2, 20500 Turku, Finland
E-mail: mathnyma@abo.fi

The ORCID identification number(s) for the author(s) of this article can be found under https://doi.org/10.1002/aesr.202300030.

[+]Present address: Institute of Physics and Astronomy, Potsdam University, Karl-Liebknecht-Str. 24-25, 14476 Potsdam-Golm, Germany

[++]Present address: Department of Mathematical, Physical and Computer Science, University of Parma, V.le delle Scienze, 7/A, 43 124 Parma, Italy

M. Pranav,[+] J. Benduhn, D. Spoltore[++]
Dresden Integrated Center for Applied Physics and Photonic Materials (IAPP) and Institute for Applied Physics
Technische Universität Dresden
Nöthnitzer Straße 61, 01187 Dresden, Germany

S. Qudsia, J.-H. Smått
Laboratory of Molecular Science and Engineering
Faculty of Science and Engineering
Åbo Akademi University
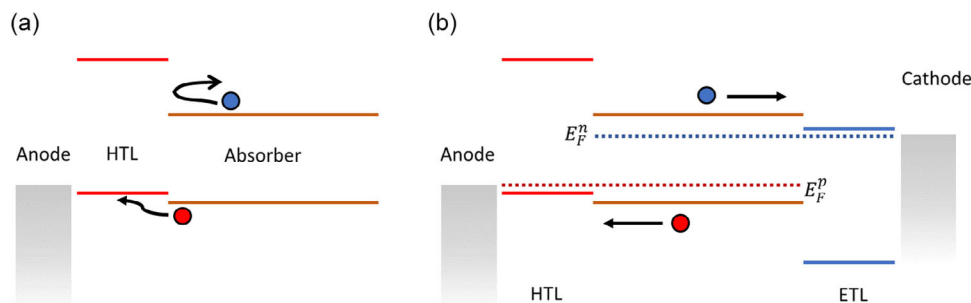Henriksgatan 2, 20500 Turku, Finland

**ADVANCED
SCIENCE NEWS**

www.advancedsciencenews.com

**ADVANCED
ENERGY & SUSTAINABILITY
RESEARCH**
Open Access

www.advenergysustres.com

Figure 1. a) A hole transporting layer (HTL) between the absorber and the contact blocks the extraction of electrons. b) Idealized schematic of the electron and hole quasi-Fermi levels (E_F^n and E_F^p) in relation to the contact work functions and energy levels of the HTL and electron transporting layer (ETL).

This means that one could make an efficient solar cell even with symmetric work function contacts, allowing for expensive metals such as gold to be replaced by cheaper alternatives.

The purpose of a charge selective interlayer is to efficiently extract one type of charge carrier while blocking the other, thereby suppressing surface recombination (**Figure 1**a). Typically, this is achieved by choosing a material with a larger bandgap than the light-absorbing material such that the valence bands (or conduction bands) are aligned, thus creating an energy barrier at the conduction bands (valence bands) (see Figure 1b). Figure 1b represents an ideal situation at flat-band conditions, in a trap-free device under illumination. In this case, it is clear that a photogenerated electron (hole) cannot be extracted at the anode (cathode) due to the high energetic barrier. As such, it is bound to be extracted at the cathode (anode) or recombine in the bulk. However, such an idealized picture is typically not valid in a real device under operation.

A more realistic schematic (although still somewhat simplified) is shown in **Figure 2**, which includes photogenerated

Figure 2. Energy-level schematic of a stack consisting of a HTL, absorber, and ETL, with an applied voltage below (upper panel) and above (lower panel) V_{bi}.

charges both in the absorber and selective layers and charge traps in the absorber and at the absorber/selective layer interface. As the transport of charge carriers is governed by drift and diffusion, it is elucidating to separately look at the situation when the applied voltage over the device, V_{appl}, is below or above V_{bi} (as the drift component goes in different directions). When $V_{appl} << V_{bi}$, the internal electric field in the active layer will drive photogenerated electrons toward the cathode and holes toward the anode. In this case, surface recombination will be negligible as the density of minority carriers in the vicinity of the contacts is low. However, when $V_{appl} >> V_{bi}$, the applied voltage will drive the photogenerated charges in the opposite direction, potentially resulting in significant densities of minority carriers at the contact and concomitant surface recombination, the magnitude of which will depend on the contact properties such as the work function and surface recombination velocity. Charges can still be extracted at the correct contact through diffusion, provided that the selective layers block minority carriers (otherwise the current will be reversed). The processes indicated by the black arrows (in particular their rates) will have a considerable effect on the V_{OC}; a V_{OC} higher than V_{bi} is not possible unless minority carriers are blocked by the selective layer.[10] It should be stressed that the actual charge carrier distributions, band bending, etc. will depend on several factors, such as the charge generation profile, charge carrier recombination rates, and transport properties. Especially at applied voltages close to the built-in potential, it is challenging to determine the actual charge carrier densities.

In most cases, the selective layers have been developed by a trial-and-error approach, and it is not conclusively clarified how a charge selective interlayer should be designed for optimal performance. What is clear is that the efficient extraction of majority carriers is of primary importance. The conductivity, defined as $\sigma = q\mu N$, where q is the electron charge, μ is the mobility, and N is the number of charges, for majority carriers (in the selective layers) needs to be high enough such that no, or a minimal, voltage drop occurs across the selective layer. This is achieved by having a high enough mobility or doping concentration or making the selective layer thin enough.[7,8] However, the processes of minority carrier surface recombination are still not well understood, and consequently, it is not clear how this surface recombination can be suppressed while maintaining a high extraction efficiency for majority carriers. It is generally assumed
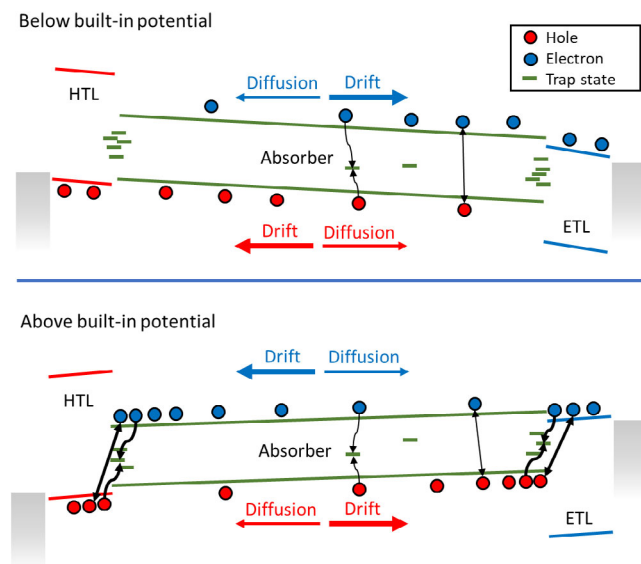
that trap-assisted recombination contributes to surface recombination; minority carriers either recombine with trapped majority carriers or are themselves trapped to subsequently recombine with free majority carriers.[12,13] However, it is unclear how the direct recombination (of free minority carriers in the active layer with free majority carriers in the selective layer) contributes to surface recombination. We note that the interface recombination (direct bimolecular recombination across the interface) for transport layer–active layer interfaces could be significant.

At an interface where electrons are minority charge carriers, the recombination current can be expressed as

$$j_R = -qS_R(n_S - n_0) \tag{1}$$

where q is the elementary charge, S_R is the surface recombination velocity, n_S is the electron concentration at the interface, and n_0 is the equilibrium carrier concentration at the contact (see Equation (2.1.6) in ref. [14]). In the case of (indirect) trap-assisted recombination, S_R depends on the thermal velocity of electrons, capture cross section, and density of the interface trap states but is independent of the concentration of both charge carrier types.[15] If the recombination across the interface is direct, then the recombination current depends on the product of both charge carriers

$$j_R \propto n_S p_S \tag{2}$$

where p_S is the hole concentration at the interface. Assuming that $j_R \approx -qS_R n_S$, S_R must then be proportional to p_S. Hence, by determining S_R, it is possible to clarify whether or not direct recombination contributes to surface recombination for a given interface.

In this article, we clarify how the surface recombination velocity of minority charges depends on the conductivity (of majority carriers) of the charge transporting layer. We use the charge extraction by a linearly increasing voltage (CELIV) technique to determine the surface recombination velocity of minority carriers in model devices based on vacuum evaporated small organic molecules. The conductivity in the transporting layer is controlled both by using materials with different mobility (intrinsic semiconductors) and by varying the doping concentration. Our results indicate that the direct bimolecular recombination between minority carriers in the active layer with majority carriers in the transporting layer can be significant and should not be overlooked. Similar results are also shown for selective layers based on metal oxides. Based on our findings, we present two different design pathways to improve the selective extraction of charges in solar cells based on low-mobility materials.

2. Results

First, we clarify how varying the charge carrier mobility in the transporting layer affects the surface recombination velocity of minority carriers. For this purpose, we use the following device structure: ITO (90 nm)/HTL p-doped with 10 wt% NDP9 (p-dopant no. 9, Novaled GmbH, Germany) (10 nm)/HTL (10 nm)/C$_{60}$ (50 nm)/BPhen (8 nm)/Al (100 nm), where ITO is indium tin oxide, doped HTL is a highly doped hole transporting layer (high enough doping to facilitate Ohmic hole injection),

Table 1. The room temperature mobilities (obtained by time-of-flight technique) and charge transfer state energies (E_{CT}, when C$_{60}$ is used as an acceptor) of the HTL materials used. The chemical formulas of the HTLs are given in the experimental section. The mobilities are taken from refs. [17–19], whereas E_{CT} are obtained from sensitive external quantum efficiency (EQE) spectra as shown in Figure S1, Supporting Information.

Material	Mobility [cm^2 Vs^{-1}]	E_{CT} [meV]
Rubrene	8×10^{-3}	1468
TAPC	3×10^{-4}	1441
Spiro-MeO-TPD	1×10^{-4}	1110
m-MTDATA	3×10^{-5}	996

HTL is the same hole transporting layer, but undoped, and BPhen is Bathophenanthroline. As HTLs, we use materials with varying energy levels, resulting in different charge transfer state energies E_{CT} (with C$_{60}$ as acceptor), and varying mobilities[16–19] (see **Table 1**).

The surface recombination velocity of minority carriers, in this case electrons, is determined using CELIV.[20] Electrons are injected from the BPhen/Al contact and driven toward the HTL using a DC offset voltage V_{OFF} (larger than the built-in voltage) in forward bias. The electron reservoir is then extracted by a linearly increasing voltage pulse in reverse bias of slope $A = -V_{max}/t_{pulse}$, where V_{max} is the maximum applied voltage and t_{pulse} is the length of the pulse. The resulting extraction current density consists of two parts: a time-independent one, $j(0)$, due to the charging of the capacitance of the device, and a time-dependent one $\Delta j(t)$, due to the extraction of the injected charge reservoir. The extracted charge Q_{extr} is given by

$$Q_{extr} = \int_0^{t_{pulse}} (\Delta j(t)) dt \tag{3}$$

The surface recombination velocity S_R is then given by

$$S_R = \frac{2\varepsilon\varepsilon_0 kT}{qQ_{extr}^2} J_D \tag{4}$$

where $\varepsilon\varepsilon_0$ is the dielectric constant, k is the Boltzmann constant, T is the temperature, and J_D is the steady-state current before the extraction pulse. Due to the high electron mobility in C$_{60}$, measurements were performed at low temperatures (50 or 100 K) in order to avoid RC effects (the time when the current transient reaches its maximum, t_{max} should be $>> RC$, where R is the resistance of the outer circuit and C is the capacitance of the device).

Figure 3a shows the extracted charge as a function of V_{OFF} for devices with four different HTLs; the corresponding extraction current transients are given in the Supporting Information. It can be seen that at low V_{OFF} there are no injected charge reservoirs because $V_{OFF} < V_{bi}$. When V_{OFF} is large enough, the extracted charge increases linearly with V_{OFF}. By then extrapolating to zero extracted charge (indicated by the arrows in Figure 3a), one can obtain the onset voltage of charge injection V_Q, which roughly corresponds to V_{bi} (assuming an Ohmic cathode). The differences in the obtained V_Q scale with E_{CT} are due to
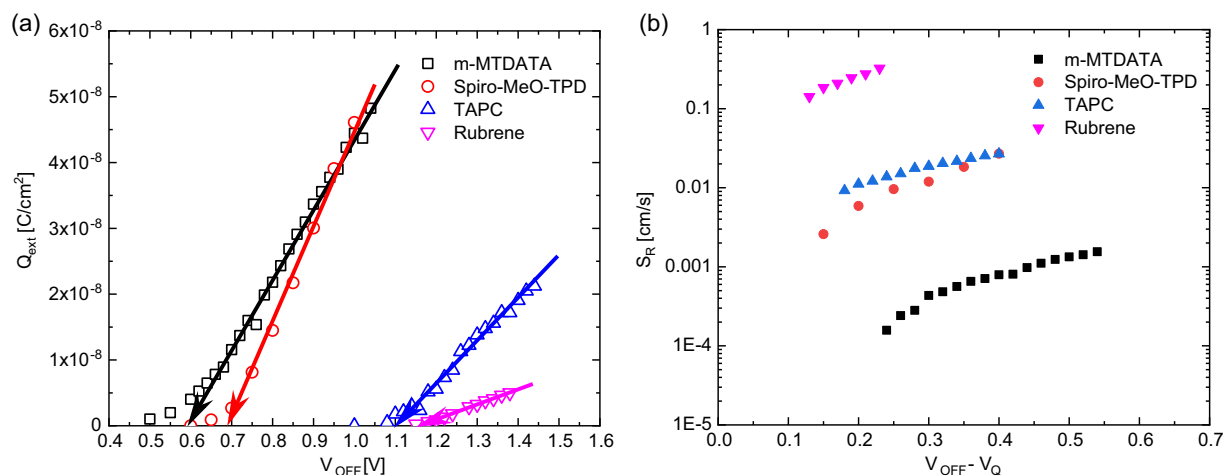
Figure 3. a) The extracted charges as a function of V_{OFF} in devices with varying HTLs. The arrows are guides to the eye, indicating V_Q (an estimate of V_{bi}). b) The corresponding S_R as a function of $V_{OFF}-V_Q$.

the difference in the quasi-Fermi levels for holes (indirectly the different highest occupied molecular orbitals of the HTL).

Figure 3b shows the S_R corresponding to Q_{ext} in Figure 3a) as a function of $V_{OFF} - V_Q$ (in order to make the comparison between different materials more straightforward). The first thing to note is that the S_R for the Spiro-MeO-TPD device and the TAPC device is almost identical, despite a significant difference in E_{CT}. The hole mobility, however, is very similar in Spiro-MeO-TPD and TAPC (see Table 1).[17,19] Rubrene, which has similar E_{CT} as TAPC but significantly higher hole mobility, has a roughly one order of magnitude higher S_R.[18] m-MTDATA, on the other hand, has the lowest hole mobility, and indeed the m-MTDATA device also has the lowest overall S_R.[19] It is clear that for the devices studied in Figure 3, an increase in the conductivity for majority carriers in the HTL by increased hole mobility correlates with an increased S_R for electrons at the HTL–active layer interface.

Another way to increase the conductivity for majority carriers in a transporting layer is by doping. In the following, we clarify the effect of varying doping concentrations in the HTL. For this purpose, we use TAPC with varying wt% of NDP9 as HTL and a C_{60}:TAPC low-donor-content (6 wt%) active layer, with the device structure ITO (90 nm)/HTL (20 nm)/C_{60}:TAPC (100 nm)/BPhen (8 nm)/Al (100 nm). We have also included devices with a 5 wt% doped TAPC layer and a 5 or 10 nm intrinsic TAPC layer. The results are summarized in **Figure 4**, the corresponding extraction current transients are found in the Supporting Information. Even though the measurements were conducted at 50 K, it was not possible to determine the S_R in devices with a higher doping concentration than 2 wt%. We also measured devices with 4, 5, 7, and 10 wt% dopant concentration in the HTL. However, S_R was too high to measure because no charge reservoir build-up could be seen. This means that S_R is larger than the effective bulk-limited transport velocity $v_D \approx \frac{\mu kT}{qd}$, where d is the C_{60}:TAPC layer thickness, i.e., electrons recombine at the HTL–active layer interface faster than they can be injected from the cathode and transported to the HTL. From the t_{max}, the mobility is $\approx 2 \times 10^{-2}$ cm^2 V$_s^{-1}$ which gives $v_D \approx 10$ cm s^{-1}.[21]
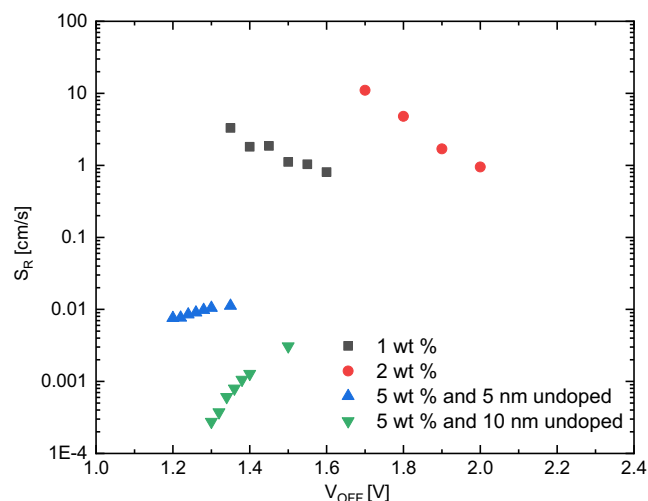

Figure 4. S_R as a function of V_{OFF} for TAPC devices with different doping levels in the HTL.

An increase in the doping concentration in the HTL leads to a higher S_R for electrons at the HTL/active layer interface. The insertion of an intrinsic HTL between the doped HTL and the active layer drastically decreases S_R, effectively acting as a "passivating layer."

It is noteworthy that S_R is not constant with varying V_{OFF}, as would be expected for purely trap-assisted recombination. In the case of undoped HTLs, S_R increases with increasing V_{OFF} whereas the opposite trend is seen for doped HTLs. Instead, we propose that, due to direct bimolecular recombination, S_R depends on the density of holes at the HTL/active layer interface. In the undoped case, the density of holes close to the HTL/C_{60} interface will be highly dependent on V_{OFF}. For $V_{OFF} < V_{bi}$, injection of holes from the anode is limited, and the hole density in the HTL is comparatively low. For $V_{OFF} > V_{bi}$, holes are injected from the anode and driven toward the HTL/C_{60}:TAPC interface where they can recombine with electrons injected from the

**ADVANCED
SCIENCE NEWS**

www.advancedsciencenews.com

**ADVANCED
ENERGY & SUSTAINABILITY
RESEARCH**
Open Access

www.advenergysustres.com

cathode, the larger the V_{OFF}, the larger the hole density in the HTL, and the larger S_R.

On the other hand, in the doped case, a depletion region forms at the anode when $V_{OFF} > V_{bi}$ with increasing width for increasing V_{OFF}. Under steady-state conditions, injected electrons (in C_{60}) recombine with doping-induced holes in the HTL. Holes then need to be replenished from the anode. However, injection of holes into the HTL will be limited by the low hole conductivity in the depletion region, effectively leading to a decreasing S_R for increasing V_{OFF} (as the depletion region width increases).

The above results show that an increase in the conductivity for majority carriers in the transporting layer leads to an increased surface recombination velocity of minority carriers due to direct bimolecular recombination across the interface—at least in devices based on organic semiconductors. It is important to note that the devices characterized here were designed to illustrate this qualitative behavior; the device performance of these devices in particular is not necessarily limited by surface recombination. The obtained S_R values are notably low; however, this is explained by the fact that the measurements were performed at low temperatures where the conductivity of the HTL is likely several orders of magnitude lower than at room temperature. Given that S_R seems to scale with the conductivity of the HTL, the S_R values at room temperature are conversely likely to be orders of magnitude higher. The J–V curves under simulated sunlight (measured at 297 K) for devices with varying doping concentration in the HTL are shown in **Figure 5 (**the dark currents and corresponding photocurrents are shown in the Supporting Information). Curiously, both the 1 and 2 wt% devices—the only devices where S_R could be determined—show clear s-shapes indicating too low conductivity in the HTL. The FF steadily improves, although the differences are quite minor for the 4 wt% and higher concentration devices. The V_{OC}, on the other hand, decreases for increasing doping concentrations in the HTL, again more or less saturating for doping concentrations above 4 wt%. However, increasing the doping concentration should lead to an increase in V_{OC}, due to an increased V_{bi}.[7]
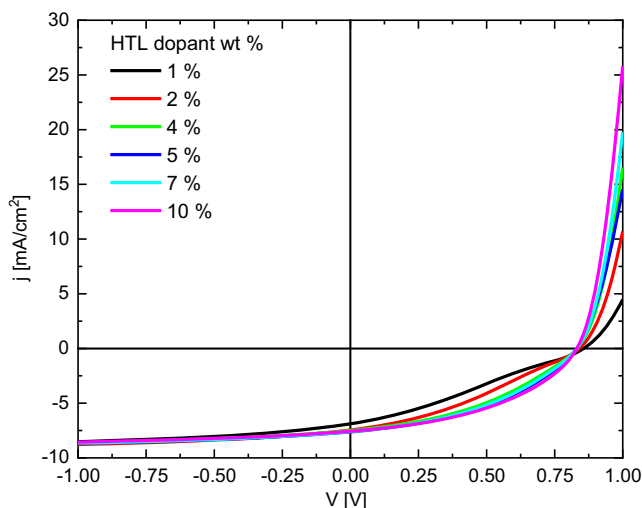
The fact that this is not seen is a clear indication that surface recombination is affecting device performance in these devices.

Another large class of materials used as selective layers is metal oxides. Most metal oxides are prone to a so-called light-soaking effect, i.e., the work function changes when exposed to UV light, making them interesting model systems for clarifying surface recombination effects.[22] It has been shown that organic solar cells (OSCs) employing TiO_2 as an electron selective layer exhibit a severe s-shape in pristine devices, which disappears with exposure to UV light. **Figure 6** shows the extraction current transients before and after UV light soaking of a hole-only ITO (90 nm)/TiO_2 (30 nm) PTB7 (340 nm)/MoO_3 (10 nm)/Ag (60 nm) device. It can be seen that the TiO_2 layer acts as an efficient hole-blocking layer before light soaking in UV light, with $S_R = 2.7 \times 10^{-6}\ cm\ s^{-1}$ in agreement with previous results.[20] However, after light soaking in UV light, no charge reservoir can be seen, and therefore the S_R cannot be determined. Again $S_R > v_D$ which means that holes are recombining at the TiO_2/PTB7 interface quicker than they can be transported through the PTB7 bulk. Note that V_{bi} most likely increases after light soaking.[22] However, the device shows no hole-blocking properties in any voltage range.

The reason why the TiO_2 layer effectively does not block holes after exposure to UV light is most likely a surface effect. Chemisorption of oxygen molecules on the surface of metal oxide films can bind free electrons from the conduction band and thereby gives rise to a depletion layer at the surface, in this case the TiO_2/PTB7 interface.[23] UV light can generate free charge carriers in the metal oxide, and recombination with the trapped electrons facilitates oxygen desorption and removal of the depletion layer at the surface, increasing surface recombination. From these results alone, it is not clear what the cause of this increase in electron density is. A drastic increase in the electron density in the TiO_2, with a concomitant increase in the direct bimolecular recombination with injected holes in the active layer, would also give the same effect. One possibility is that the photocatalytic effect causes the TiO_2 layer to become highly doped—this would explain both the fact that holes are not blocked at the TiO_2/PTB7 interface and the decrease in the effective work function (increase of V_{bi}). However, UV–vis–NIR absorption measurements of TiO_2 films show no difference before and after UV treatment, indicating that there is no drastic conductivity increase in the bulk due to possible doping of the TiO_2 layer (see Figure S10, Supporting Information). Another possibility is that UV light causes the ITO-work function to decrease, making the ITO/TiO_2-contact Ohmic for electrons, thus facilitating electron injection.[24]

3. Discussion

The terms selective layers, extraction layers, passivation layers, transporting layers, and blocking layers are used almost interchangeably in the fields of organic and perovskite photovoltaics. These terms often refer to the same thing; thin interlayers used to facilitate selective charge extraction and suppress surface recombination. However, it is important to remember that these terms are not synonymous. For example, a passivation layer is not necessarily a transporting layer; if the passivation layer is thin
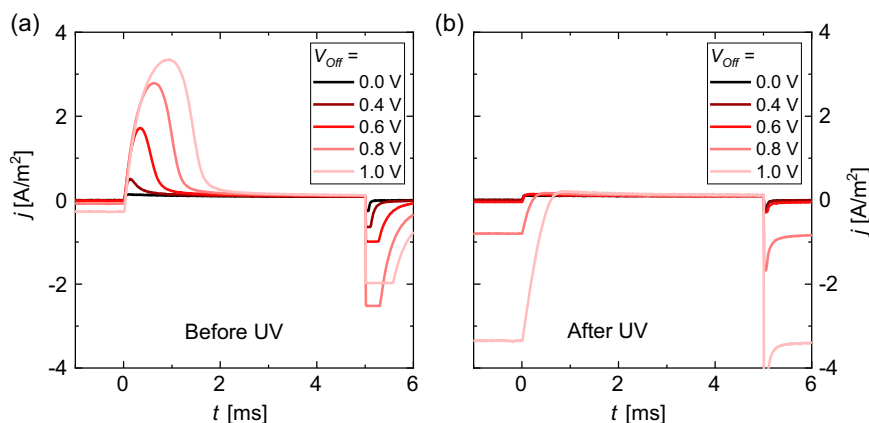

Figure 5. J–V curves measured under simulated sunlight for ITO (90 nm)/ TAPC *p*-doped with varying wt% NDP9 (20 nm)/C_{60}:TAPC (6 wt%) (100 nm)/BPhen (8 nm)/Al (100 nm) devices.

Figure 6. a) The surface recombination velocity before UV treatment is $S_R = 2.7 \times 10^{-6}$ cm s^{-1} (average from $V_{Off} = 0.6$ V to $V_{Off} = 1.4$ V). b) No reservoir is seen after UV treatment meaning that the TiO$_2$ interlayer acts as a perfect electron collecting contact for the device. The measurement is in this case limited by the effective bulk limited transport velocity $v_D \approx \frac{\mu k T}{q d} \approx 0.08$ cm s^{-1}, yielding a lower limit to S_R after UV treatment.

enough, charge carriers can tunnel rather than be transported through them.[25,26] More importantly, as the results presented here demonstrate, a hole transporting (extraction) layer is not the same as an electron blocking layer. As shown, an interlayer with high conductivity for holes effectively does not block electrons due to interface recombination. This has direct consequences for optimizing the selective extraction of charges in real devices.

Surface recombination in organic and perovskite solar cells is typically assumed to be trap-assisted. In this case, surface recombination can be reduced simply by reducing the density of trap states (reducing the amount of defects, etc.). Reducing the number of trap states will always have a positive effect on device performance, regardless of whether the traps are located in the active layer bulk, in the selective layer, or at the interfaces. The critical question is how to reduce the density of trap states. However, we have shown that interface recombination across the absorber layer/transporting layer interface is another potential cause of surface recombination. This means that reducing trap states is a perhaps necessary, but not sufficient requirement to minimize surface recombination. In order to minimize surface recombination, one also needs to minimize interface recombination, which is challenging because a high majority carrier conductivity in the selective layer (necessary for a high FF and V_{OC}) can result in significant interface recombination across the selective layer/active layer interface. In the following, we propose two design principles to suppress surface recombination of minority carriers while maintaining an efficient majority carrier extraction.

For any recombination process, the recombination rate R can be expressed as $R = C_r N^\alpha$, where C_r is a recombination constant, N is the density of charge carriers, and α is the reaction order, which depends on the type of recombination in question. For a particular recombination process (α assumed fixed), there are thus two possible ways of reducing R; lowering either C_r or N.

3.1. Charge Carrier Distribution—The Role of Built-In Voltage

The perhaps most straightforward way to reduce interfacial recombination at the selective layer/active layer interface, at least

in theory, is to reduce the density of minority carriers at this interface. As discussed earlier, the carrier distributions under operation are governed by drift and diffusion and are a fairly intricate interplay between several parameters such as the generation profile, charge carrier transport, and recombination. This makes it challenging to control the carrier distribution via device design. However, one possible way of achieving a beneficial charge distribution is by increasing V_{bi}. The role of V_{bi} in the selective extraction of charges in organic and perovskite solar cells has been a recurring topic in the literature.[6,7,11,26–28] Our results indicate that hole transporting layers with a high conductivity do not block electrons when $V_{appl} > V_{bi}$. This shows that in devices with charge transporting layers, the operating voltage should be below V_{bi} to avoid interface recombination, i.e., increasing V_{bi} could make it possible to shift the maximum power point toward higher voltages. This supports the view that a high V_{bi} is beneficial for device performance. However, any positive effect is likely to be highly device-dependent. The fact that most highly efficient solar cells have a higher V_{bi} than the applied voltage at maximum power point explains why it is possible to have both highly conductive charge transporting layers and low voltage losses to surface recombination.

3.2. Passivation Layers

Passivation layers of various types have been frequently used in the literature, in particular in perovskite solar cells. The rationale behind using a passivation layer is that it "passivates" (i.e., deactivates) traps at the selective layer/active layer (or active layer/contact) interface, which results in reduced surface recombination. In the case of trap-assisted recombination, the recombination coefficient is dependent on the trap density (and trap depth), i.e., reducing the trap density reduces the recombination coefficient and thus the recombination rate. However, our results indicate another benefit of using a thin interfacial layer between the charge transporting layer and the absorber, namely suppression of the direct bimolecular recombination between majority carriers in the transport layer and minority carriers in the

absorber. This is demonstrated in Figure 4, where an intrinsic semiconductor layer between the doped HTL and the absorber leads to orders of magnitude reduction in S_R. However, the properties of this passivation layer need to be carefully chosen so as not to compromise majority carrier extraction. For example, using an intrinsic transporting layer will not necessarily improve overall device performance (as demonstrated in Figure 4); if the layer is too thick or the mobility too low, majority carrier extraction will be compromised.[7,8] However, most passivation layers do not actually transport charge. Instead, majority carriers are transferred from the absorber to the transporting layer by tunneling across the passivation layer. This means that a passivation layer always needs to be thin, which might prove to be a challenge for scale-up.

4. Conclusions

We have clarified how the surface recombination velocity of minority charges at the charge transporting layer/active layer interface depends on the conductivity (of majority carriers) of the charge transporting layer. Our results show that, due to direct bimolecular recombination across the interface, charge transporting layers that efficiently transport majority carriers do not block minority carriers. In any solar cell with charge transporting layers, all photogenerated carriers have to be transported through the charge transporting layers in order to be extracted. The HTLs and ETLs will thus have large charge carrier densities originating from photogeneration in the bulk, regardless of whether or not they are doped. This also means that surface recombination effectively involves mainly photogenerated charges (although majority carriers have been transferred to the charge transporting layer). In order to avoid surface recombination in devices with charge transporting layers, one has to minimize the interfacial recombination, for example, by increasing V_{bi} or employing a thin passivation layer at the transporting layer/active layer interface.
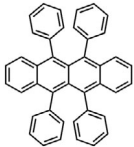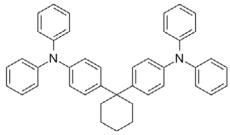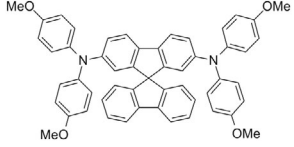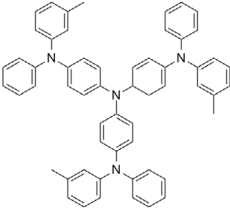
5. Experimental Section

Device Fabrication: The devices were fabricated according to our previous work. The description is reproduced here for completeness.[29] All devices investigated in this work were constructed by a thermal evaporation vacuum system with a base pressure of less than 10^{-7} mbar. Before deposition, ITO substrates (Thin Film Devices Inc., USA) were cleaned for 15 min in different ultrasonic baths with NMP solvent, deionized water, and ethanol, followed by O_2 plasma for 10 min. The organic materials were purified 1 or 2 times via thermal sublimation. A series of shadow masks and mobile shutters were utilized to control device layout and thickness variation. The effective active area was defined by the geometrical overlap of the bottom and top contact (four different areas were used: 6.44, 3.22, 1.61, and 0.81 mm²). After fabrication, all devices were encapsulated by gluing a transparent glass on top of the device utilizing an epoxy resin (Nagase ChemteX Corp., Japan) cured by UV light. To hinder degradation, a moisture getter (Dynic Ltd., UK) was inserted between the top contact and the glass.

Materials: **Table 2**.

Sensitive EQE Measurements: The sensitive EQE measurements were performed according to previous works, the experimental protocol is reproduced here for completeness.[30] The light of a quartz halogen lamp (50 W) was chopped at 140 Hz and coupled into a monochromator (Newport Cornerstone 260 1/4 m). The resulting monochromatic light

Table 2. The chemical formulas of the used HTLs.

No.	Donor (supplier)	Structure and chemical name
1	Rubrene (Sensient)	5,6,11,12-tetraphenyl-tetracene
2	TAPC (Sensient)	1,1-bis[4-(N,N-di-p-tolylamino)phenyl]cyclohexane
3	Spiro-MeO-TPD (Lumtec)	2,7-bis[N,N-bis(4-methoxy-phenyl)amino]9,9-spiro-bifluorene
4	m-MTDATA (Lumtec)	4,4′,4″-tris(3-m-tolyl-phenylamino)-triphenylamine

was focused onto the OSC, and its current under short-circuit conditions was fed to a current preamplifier before it was analyzed with a lock-in amplifier (Signal Recovery 7280 DSP). The time constant of the lock-in amplifier was chosen to be 1 s and the amplification of the preamplifier was increased to resolve low photocurrents. The external quantum efficiency (EQE) was determined by dividing the photocurrent of the OSC by the flux of incoming photons, which was measured using a calibrated Si and InGaAs photodiode (FDS100-CAL and FGA21-CAL, Thorlabs). According to ref. [31], the energy of the charge transfer state E_{CT} was obtained from the low energy tail of the sensitively measured EQE spectra.

Supporting Information

Supporting Information is available from the Wiley Online Library or from the author.

Acknowledgements

Conflict of Interest

The authors declare no conflict of interest.

Data Availability Statement

Research data are not shared

Keywords

charge selective interlayers, surface recombination, thin-film solar cells

[1] NREL, *Research Cell Efficiency Record*, https://www.nrel.gov/pv/assets/pdfs/cell-pv-eff-emergingpv-rev220630.pdf (Accessed: November 2022).

[2] M. B. Johnston, L. M. Herz, *Acc. Chem. Res* **2016**, *49*, 146.

[3] M. Nyman, O. J. Sandberg, W. Li, S. Zeiske, R. Kerremans, P. Meredith, A. Armin, *Solar RRL* **2021**, 2100018.

[4] S. Wilken, D. Scheunemann, S. Dahlström, M. Nyman, J. Parisi, R. Österbacka, *Adv. Electron. Mater.* **2021**, 2001056.

[5] R. Sorrentino, E. Kozma, S. Luzzati, R. Po, *Energy Environ. Sci.* **2021**, *14*, 180.

[6] J. F. Butscher, S. Intorp, J. Kress, Q. An, Y. J. Hofstetter, N. Hippchen, F. Paulus, U. H. F. Bunz, N. Tessler, Y. Vaynzof, *ACS Appl. Mater. Interfaces* **2020**, *12*, 3572.

[7] C. Ahläng, M. Nyman, R. Österbacka, *Phys. Rev. Appl.* **2021**, *16*, 014041.

[8] V. M. Le Corre, M. Stolterfoht, L. Perdigón Toro, M. Feuerstein, C. Wolff, L. Gil-Escrig, H. J. Bolink, D. Neher, L. J. A. Koster, *ACS Appl. Energy Mater.* **2019**, *2*, 6280.

[9] S. Pisoni, M. Stolterfoht, J. Löckinger, T. Moser, Y. Jiang, P. Caprioglio, D. Neher, S. Buecheler, A. N. Tiwari, *Sci. Technol. Adv. Mater.* **2019**, *20*, 786.

[10] O. J. Sandberg, A. Sundqvist, M. Nyman, R. Österbacka, *Phys. Rev. Appl.* **2016**, *5*, 044005.

[11] U. Würfel, A. Cuevas, P. Würfel, *IEEE J. Photovoltaics* **2015**, *5*, 461.

[12] J. Haddad, B. Krogmeier, B. Klingebiel, L. Krückemeier, S. Melhem, Z. Liu, J. Hüpkes, S. Mathur, T. Kirchartz, *Adv. Mater. Interfaces* **2020**, *7*, 2000366.

[13] J. Vollbrecht, V. V. Brus, *Org. Electron.* **2020**, *86*, 105805.

[14] O. J. Sandberg, Ph.D. Thesis, Åbo Akademi University (**2018**)

[15] J. Nelson, in *The Physics Of Solar Cells*, Imperial College Press and Distributed by World Scientific Publishing Co., London **2003**.

[16] D. Spoltore, A. Hofacker, J. Benduhn, S. Ullbrich, M. Nyman, O. Zeika, S. Schellhammer, Y. Fan, I. Ramirez, S. Barlow, M. Riede, S. Marder, F. Ortmann, K. Vandewal, *J. Phys. Chem. Lett.* **2018**, *9*, 5496.

[17] D. Poplavskyy, J. Nelson, *J. Appl. Phys.* **2013**, *93*, 341.

[18] H. H. Fong, S. K. So, W. Y. Sham, C. F. Lo, Y. S. Wu, C. H. Chen, *Chem. Phys.* **2004**, *298*, 119.

[19] M. Aonuma, T. Oyamada, H. Sasabe, T. Miki, C. Adachi, *Appl. Phys. Lett.* **2007**, *90*, 183503.

[20] O. J. Sandberg, S. Sandén, A. Sundqvist, J.-H. Smått, R. Österbacka, *Phys. Rev. Lett.* **2017**, *118*, 076601.

[21] G. Juška, K. Arlauskas, M. Viliunas, J. Kocka, *Phys. Rev. Lett.* **2000**, *84*, 4946.

[22] A. Sundqvist, O. J. Sandberg, M. Nyman, J.-H. Smått, R. Österbacka, *Adv. Energy Mater.* **2016**, *6*, 1502265.

[23] S. Wilken, J. Parisi, H. Borchert, *J. Phys. Chem. C* **2014**, *118*, 19672.

[24] S. Schäfer, A. Petersen, T. A. Wagner, R. Kniprath, D. Lingenfelser, A. Zen, T. Kirchartz, B. Zimmermann, U. Würfel, X. Feng, T. Mayer, *Phys. Rev. B* **2011**, *83*, 165311.

[25] K. Ding, S. R. Forrest, *Phys. Rev. Appl.* **2020**, *13*, 054046.

[26] M. Pranav, J. Benduhn, M. Nyman, S. M. Hosseini, J. Kublitski, S. Shoaee, D. Neher, K. Leo, D. Spoltore, *ACS Appl. Mater. Interfaces* **2021**, *13*, 12603.

[27] Gert-Jan A. H. Wetzelaer, Paul W. M. Blom, *ACS Appl. Mater. Interfaces* **2022**, *14*, 7523.

[28] M. Pranav, J. Benduhn, M. Nyman, S. M. Hosseini, J. Kublitski, S. Shoaee, D. Neher, K. Leo, D. Spoltore, *ACS Appl. Mater. Interfaces* **2022**, *14*, 7527.

[29] S. Xing, V. C. Nikolis, J. Kublitski, E. Guo, X. Jia, Y. Wang, D. Spoltore, K. Vandewal, H. Kleemann, J. Benduhn, K. Leo, *Adv. Mater.* **2021**, 2102967.

[30] J. Benduhn, K. Tvingstedt, F. Piersimoni, S. Ullbrich, Y. Fan, M. Tropiano, K. A. McGarry, O. Zeika, M. K. Riede, C. J. Douglas, S. Barlow, S. R. Marder, D. Neher, D. Spoltore, K. Vandewal, *Nat. Energy* **2017**, *2*, 17053.

[31] K. Vandewal, K. Tvingstedt, A. Gadisa, O. Inganäs, J. V. Manca, *Phys. Rev. B* **2010**, *81*, 125204.